A Generalization of Theory for Two-Dimensional Fluorescence Recovery after Photobleaching Applicable to Confocal Laser Scanning Microscopes

Minchul Kang,[†] Charles A. Day,[†] Kimberly Drake,[†] Anne K. Kenworthy,[†‡*] and Emmanuele DiBenedetto[†§*]
[†]Department of Molecular Physiology and Biophysics, and [‡]Department of Cell and Developmental Biology, Vanderbilt University School of Medicine, Nashville, Tennessee, and [§]Department of Mathematics, Vanderbilt University, Nashville, Tennessee

ABSTRACT Fluorescence recovery after photobleaching (FRAP) using confocal laser scanning microscopes (confocal FRAP) has become a valuable technique for studying the diffusion of biomolecules in cells. However, two-dimensional confocal FRAP sometimes yields results that vary with experimental setups, such as different bleaching protocols and bleaching spot sizes. In addition, when confocal FRAP is used to measure diffusion coefficients (D) for fast diffusing molecules, it often yields D-values that are one or two orders-of-magnitude smaller than that predicted theoretically or measured by alternative methods such as fluorescence correlation spectroscopy. Recently, it was demonstrated that this underestimation of D can be corrected by taking diffusion during photobleaching into consideration. However, there is currently no consensus on confocal FRAP theory, and no efforts have been made to unify theories on conventional and confocal FRAP. To this end, we generalized conventional FRAP theory to incorporate diffusion during photobleaching so that analysis by conventional FRAP theory for a circular region of interest is easily applicable to confocal FRAP. Finally, we demonstrate the accuracy of these new (to our knowledge) formulae by measuring D for soluble enhanced green fluorescent protein in aqueous glycerol solution and in the cytoplasm and nucleus of COS7 cells.

INTRODUCTION

Fluorescence recovery after photobleaching (FRAP) was developed using a wide-field microscope equipped with a static laser in the 1970s to investigate the diffusion of proteins in membranes. The theory for FRAP with a static laser, which we will refer to herein as conventional FRAP, is well described (1). As commercial confocal laser scanning microscopes with controlled photobleaching capabilities have become widely available, confocal FRAP has become a valuable technique to study the mobility of cellular components (2–4).

Confocal FRAP differs in several important ways from conventional FRAP. In conventional FRAP, a static laser with either a Gaussian profile or a uniform disk profile defines both the bleaching region of interest (ROI) and the observation ROI, and switching between bleaching mode and observation mode is carried out by rapidly attenuating the laser intensity. On the other hand, in confocal FRAP, a scanning laser with a fixed beam radius is used to image the specimen and perform the photobleach. This has both pros and cons. Since the bleaching ROIs are filled by lines of laser scans, noncircular ROIs can easily be considered. Even better, the bleaching ROI may not necessarily be the same as the observation ROI, allowing for direct visualization of the movement of bleached molecules away from the bleach ROI into the surrounding area (5). However, for confocal FRAP using laser scanning confocal microscopes, the scanning time is not infinitesimally small and it takes a relatively long time for a large ROI to be scanned.

Due to the long scanning time of confocal laser scanning microscopes (approximately seconds), when conventional FRAP analysis is applied to confocal FRAP measurements for fast diffusing molecules like soluble enhanced green fluorescent protein (EGFP), underestimated values of D are often obtained (6,7). Even worse, these values vary as a function of bleaching spot sizes and bleaching scan times (6,8). Recent studies indicate that the underestimation of D is mainly due to the relatively long bleaching time and corresponding diffusion that occurs during photobleaching (6,7).

It was further demonstrated that underestimation of D for fast diffusing proteins in confocal FRAP can be corrected by considering diffusion during photobleaching by generating mathematical models incorporating realistic initial conditions (7,9), while the conventional formalism (1) is still valid for slowly diffusing molecules. However, the functional form of currently available confocal FRAP formula (7,9) differs considerably from that of conventional FRAP analysis, making it difficult to apply a theory based on the conventional FRAP analysis directly to confocal FRAP data. Thus, we sought to develop a simple yet generalized FRAP theory for two-dimensional circular ROIs that encompasses the features of both conventional FRAP and confocal FRAP and that is applicable to both rapidly and slowly diffusing molecules.

MATERIALS AND METHODS

A glossary of symbols appearing in this study can be found in Supporting Material A.

Conventional FRAP theory

In conventional FRAP, FRAP formulae come in two different forms based on the laser profiles: a Gaussian laser and a uniform disk laser profile (1). For the

Submitted October 28, 2008, and accepted for publication June 16, 2009.

*Correspondence: anne.kenworthy@vanderbilt.edu or em.diben@vanderbilt.edu

Editor: Elliot L. Elson.

0006-3495/09/09/1501/11 $2.00

doi: 10.1016/j.bpj.2009.06.017

case of a Gaussian-type detection laser profile (I_{r_n}), the formulation of the conventional FRAP formula for fluorescence recovery in time ($F(t)$) is given by

$$F(t) = q\iint_{R^2}[\epsilon I_{r_n}(x,y)]\,C(x,y,t)dxdy, \quad (1)$$

$$I_{r_n}(x,y) = \frac{2I_0}{\pi r_n^2}\exp\left(-\frac{2(x^2+y^2)}{r_n^2}\right), \quad (2)$$

where q is the quantum yield of the fluorophores, and $\epsilon I_{r_n}(x,y)$ is the attenuated excitation laser ($\varepsilon \ll 1$) with nominal radius r_n, defined as the half-width at e^{-2} height of the maximal laser intensity (I_0). For a uniform-disk-type detection laser profile, $I^*_{r_n}(x,y)$, we consider

$$I^*_{r_n}(x,y) = \begin{cases} \dfrac{I_0}{\pi r_n^2} & \text{if } x^2+y^2 \le r_n^2 \\ 0 & \text{othewise} \end{cases}. \quad (3)$$

in the position of $I_{r_n}(x,y)$ in Eq. 1.

$C(x, y, t)$ describes the evolution of the fluorescence molecule concentration in space and time. In general, $C(x, y, t)$ is a solution of mathematical models. If pure diffusion with a diffusion coefficient, D, is assumed, then $C(x, y, t)$ in two dimensions can be represented as

$$C(x,y,t) = \frac{1}{4\pi Dt}\iint_{R^2} C(x',y',0) \times \exp\left(-\frac{\left((x-x')^2+(y-y')^2\right)}{4Dt}\right)dx'dy', \quad (4)$$

where the initial postbleach profile can be approximated by an exponential function of the Gaussian laser profile, I_{r_e} (1,6–9):

$$C(x,y,0) = C_i\exp\left[-K\exp\left(-\frac{2(x^2+y^2)}{r_e^2}\right)\right]. \quad (5)$$

Here, K is a bleaching-depth parameter and C_i is prebleach steady-state fluorescence molecule concentration. In the conventional FRAP theory, Eq. 1 for a Gaussian laser is represented as (1)

$$F(t) = F_i\sum_{m=0}^{\infty}\frac{(-K)^m}{m!(1+m[2t/\tau_D+1])}, \quad (6)$$

where $\tau_D = r^2/(4D)$. In addition, for the uniform disk laser profile, Eq. 1 can be reduced to (10)

$$F(t) = \exp\left(-\frac{2\tau_D}{t}\right)\left[\mathbf{I}_0\left(\frac{2\tau_D}{t}\right)+\mathbf{I}_1\left(\frac{2\tau_D}{t}\right)\right], \quad (7)$$

where $\mathbf{I}_k$ are modified Bessel functions ($k = 0, 1$).

EGFP in Bis:Acrylamide gel and aqueous glycerol solution

Purified enhanced green fluorescent protein (EGFP) (courtesy of D. Piston) was immobilized in a 20% Bis:Acrylamide gel by mixing EGFP with the Bis:Acrylamide solution before the addition of ammonium persulfate and N, N, N′, N′-tetramethylethylenediamine. A final EGFP concentration of 100 nM was achieved. Immediately following the addition of the polymerizing agents, a small aliquot was pipetted under glass cover slides on microscope slides. FRAP was performed 5–30 min after the polymerization of the Bis:Acrylamide gel.

For measurements of EGFP diffusion in solutions of aqueous glycerol, purified EGFP was suspended into dH20 and glycerol (40, 50, and 70% glycerol by mass) to a final EGFP concentration of 0.8 μM.

Cells and transfections

COS7 cells (ATCC, Manassas, VA) were plated in Dulbecco's modified Eagle's medium +10% fetal bovine serum onto glass cover slides two days before FRAP. Cells were maintained at 37°C and 5% CO_2. Cells were transfected with a p53-EGFP plasmid (11) or EGFP construct (Clontech, Mountain View, CA) using FuGENE 6 transfection reagent (Roche Applied Science, Hoffmann-La Roche, Basel, Switzerland) one day before FRAP. For FRAP experiments, the cells were mounted in phenol-red free Dulbecco's modified Eagle's medium supplemented with 25 mM HEPES and 1 mg/mL bovine serum albumin.

Confocal FRAP

FRAP experiments were carried out on a Zeiss LSM 510 confocal microscope (Carl Zeiss MicroImaging, Jena, Germany) using filter sets provided by the manufacturer. Imaging was performed using a 40 × 1.3 NA Zeiss Plan-Neofluar objective at 4 × zoom. EGFP was excited at 488 nm. The confocal pinhole was set to 1.01 Airy units and images were collected, with no line averaging, at 1% transmission. Experiments were performed using a circular bleach ROI centered within a rectangular or square observation ROI.

Confocal laser scanning profile on 20% Bis:Acrylamide gel

Data were collected over an 80 × 30 pixel (9.0 μm × 3.4 μm) observation ROI containing a circular bleach ROI 20 pixels (2.3 μm) in diameter. EGFP was bleached at 488 nm for 10 scans (0.425 s) using an Argon laser (Zeiss LSM 510 confocal microscope, Carl Zeiss MicroImaging, Jena, Germany) at 25% power. Pre- and postbleach images were collected at a lower laser power. Data were collected for 70 scans. FRAP measurements were carried out at 22°C.

EGFP diffusion in the aqueous glycerol solutions

Data were collected using a square observation ROI of 70 × 70 pixel (7.7 μm × 7.7 μm) containing a circular bleach ROI of 20 pixels (2.2 μm) in diameter or a 50 × 50 pixel square observation ROI (5.5 μm × 5.5 μm) with a circular bleach ROI 10 pixels (1.1 μm) in diameter. EGFP was bleached at 488 nm for 40 scans using an Argon laser (Zeiss LSM 510 confocal microscope, Carl Zeiss MicroImaging) at full power. The final bleach time was 0.444–1.600 s, depending on ROI size and number of bleaching iterations. Pre- and postbleach images were collected at a lower laser power. Data were collected for 117 scans. FRAP measurements were carried out at 30°C using a stage heater (Pecon GmbH, Erbach, Germany).

EGFP diffusion in COS7 cells

Data were collected at 22°C using a square observation ROI of 70 × 70 pixel (7.7 μm × 7.7 μm) containing a circular bleach ROI 20 pixels (2.2 μm) in diameter or a 50 × 50 pixel square observation ROI (5.5 μm × 5.5 μm) with a circular bleach ROI 10 pixels (1.1 μm) in diameter. For bleaching, the 488 laser power was increased to 100% and the bleach region was scanned repeatedly either 20 times or 40 times. This resulted in the following bleach times: 20 scans, 0.44 s for the 10 pixel bleach spot and 0.87 s for the 20 pixel bleach spot; and 40 scans, 0.79 s for the 10 pixel bleach spot and 1.6 s for the 20 pixel bleach spot. During recovery, images were collected every 0.098 s for the 50 × 50 pixel observation ROI or 0.14 s for the 70 × 70 pixel observation ROI for a total of 9.407 s or 13.02 s, respectively. FRAP measurements were carried out at 22°C.

Normalization of recovery curves

Confocal FRAP recovery curves were generated by plotting the mean fluorescence intensity within the nominal bleach ROI over time. The first image collected after the bleach was set as $t = 0$. The recovery curves were normalized by dividing by the average fluorescence intensity of the observation

ROI for the first prebleach image (F_i). No background subtraction was performed. Since the detector blinking has been reported as negligible in circular region photobleaching (9), no adjustment was made to the FRAP data to correct for this effect.

Laser profiles and effective radius (r_e)

To generate initial postbleach profiles, fluorescence intensities from the first postbleach image were measured along two diagonals of the observation ROIs. The fluorescence intensities were normalized by dividing by the mean prebleach fluorescence intensity as described above. The mean was calculated for 10 normalized initial postbleach fluorescence intensity profiles from each set of experimental parameters. The mean profiles were then fitted by

$$f(x,y) = \exp\left(-K\exp\left(-\frac{2(x^2+y^2)}{r_e^2}\right)\right) \qquad (8)$$

with the bleaching depth parameter (K) and an effective radius (r_e) as fitting parameters to minimize the sum of mean-square errors.

Data fitting and weighted residual

The FRAP curves were normalized by the mean prebleach fluorescence intensity (F_i) and the mean of 10 normalized FRAP data sets was used for data fitting. Data fitting was carried out by minimizing a weighted residual between averaged FRAP data from 10 experiments ($F_{Data}(t)$) and a theoretical FRAP curve ($F(t)$), where the weighted residual is defined by

$$\|F_{Data}(t) - F(t)\| = \int_0^s \frac{|F_{Data}(\xi) - F(\xi)|}{\xi + \int_0^s F_{Data}(\zeta)d\zeta} d\xi, \qquad (9)$$

where s is the last timepoint of FRAP data.

In Eq. 9, the difference $|F_{Data}(\xi) - F(\xi)|$ was weighted by time (ξ) so that differences in the early time period contribute more to the residual. To remove a singularity at $t = 0$, the total area of FRAP data ($\int_0^s F_{Data}(\zeta)d\zeta$) was added in the denominator as a normalization. By doing this, the goodness of fitting can be compared from one data set to another.

RESULTS

Dependence of D_n on experimental setup in confocal FRAP

To determine the extent to which diffusion during photobleaching impacts measurements of D for fast diffusing molecules using confocal FRAP, we performed FRAP measurements for two soluble proteins. The first, EGFP, is an example of a protein that does not interact with cellular components. The second, p53-EGFP, is a DNA-binding protein that undergoes weak interactions with chromatin under steady-state conditions, causing it to diffuse more slowly than predicted by the Stokes-Einstein equation (11).

To be able to visualize the extent to which bleached molecules diffuse during the photobleaching, we imaged a square region of interest, within which we defined a circular region to photobleach. To determine how much the measured D depends on experimental conditions, we performed experiments using circular bleaching spots with either a 0.55- or 1.1-μm nominal bleach radius r_n for either 20 or 40 photobleaching scans at 100% laser power.

Representative images from confocal FRAP experiments for EGFP and p53-EGFP are shown in Fig. 1. When the two proteins were photobleached under identical conditions, the boundary of the bleaching region for p53-EGFP was well defined, while no well-defined boundary was observed for EGFP in either the nucleus or cytosol (Fig. 1 *A*). However, even for p53-EGFP the bleached region appeared significantly larger than the region selected for photobleaching. This indicates that 1), diffusion during photobleaching occurs for both proteins; and that 2), diffusion of EGFP is faster than that of p53-EGFP (since the extent of diffusion during the photobleach is greater for EGFP than for p53-EGFP).

We next generated recovery curves from such experiments and used them to calculate halftimes of recovery. We then fit the resulting recovery curves with a conventional FRAP formula (Eq. 6) and calculated the resulting D assuming the nominal bleach radius (D_n). While the fits to the FRAP curves appear reasonable (Fig. 1 *B*, *solid lines*), the resulting D_n values were much smaller than previously reported in the literature by fluorescence correlation spectroscopy (Fig. 1 *D*). Thus, failing to correct for diffusion during the photobleach leads to gross underestimates of D_n. And thus, while these data are clearly characteristic of a diffusional recovery, the reported D_n using this method is erroneous.

To determine how much the experimental setup affects the apparent D_n values, we compared D_n values as a function of several different bleach spot sizes and numbers of bleaching scans. In agreement with other studies (8), we found that D_n for EGFP was dependent on both of these experimental parameters (Fig. 1 *D*). In particular, D_n values obtained by the conventional FRAP analysis were larger for larger bleaching ROIs. The dependence on the number of bleaching scans was relatively weak, possibly due to the use of >20 iterations of photobleaching scans (6). Nevertheless, for more bleaching scan iterations, smaller D_n values tended to be obtained as reported in Weiss (6). These data indicate that under the conditions of these experiments, the conventional FRAP formula is not applicable and yields inaccurate results. We therefore next sought how to generate a FRAP formula that would accommodate these intrinsic features of confocal FRAP measurements.

Derivation of a generalized FRAP formula that accounts for diffusion during the photobleach

As illustrated above, a major factor contributing to the underestimation of D and dependence of D on experimental conditions in confocal FRAP is diffusion during the photobleach that is a result of the finite time required to scan the specimen (6,7). Several methods have been proposed to correct for this effect. One of these, proposed by Braga et al. (7), addresses this issue by incorporating an effective radius as well as a nominal bleach radius into the FRAP model. In addition, this model assumes that the detector profile is a step function (uniform laser profile) that is zero outside of the region that

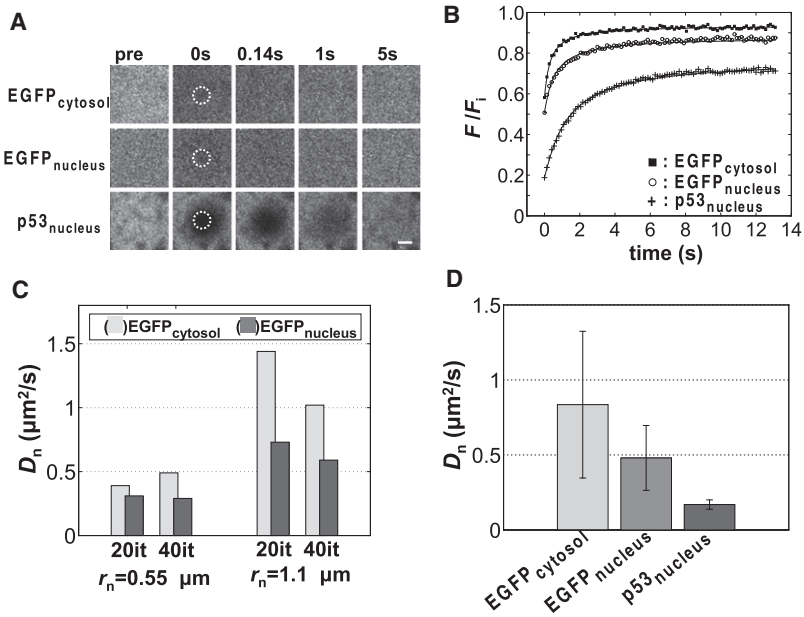

FIGURE 1 Visualization of diffusion during the photobleach in confocal FRAP and dependence of D on experimental parameters. (*A*) Representative images taken from confocal FRAP measurements of a fast diffusing molecule (EGFP) and a more slowly diffusing molecule (p53-EGFP). The bleach spot (*dashed circle*, $r_n = 1.1$ μm) was scanned 20 times using 100% laser power before acquisition of the first postbleach image. Bar = 2 μm. (*B*) Comparison of confocal FRAP curves for EGFP in the cytosol and the nucleus and p53-EGFP in the nucleus. Data represent the averaged FRAP data for 10 cells from a representative experiment. (*C*) Dependence of D on experimental parameters for EGFP in the cytosol and the nucleus. (*D*) Comparison of D-values of EGFP and p53-EGFP in COS-7 cells as measured using the conventional FRAP formula (Eq. 6). Each bar shows the mean ± SD for one of four different combinations of FRAP setups (20 or 40 photobleaching iterations, 0.55-μm or 1.1-μm bleaching ROI radius).

was bleached (7,12). This reflects the fact that in confocal FRAP, fluorescence recovery is monitored by scanning the laser across the sample and then averaging the fluorescence within the bleaching ROI. This is different from the case where the bleaching and detection laser profiles are both Gaussian, as is typically assumed in analysis of conventional FRAP measurements where the same laser is used to perform the photobleach and then to monitor the fluorescence in the bleach ROI.

As mentioned above, Braga and colleagues incorporated these two features into their confocal FRAP model by assuming a Gaussian laser profile with an effective radius r_e of the photobleaching laser and a uniform disk detection laser profile (7). In this approach, the averaged fluorescence intensities over a bleach ROI with a radius r_n are represented as

$$\tilde{F}(t) = \frac{1}{\pi r_n^2 C_i}\int\int_{x^2+y^2\le r_n^2} C(x,y,t)dxdy, \qquad (10)$$

where $C(x, y, t)$ is given by Eqs. 4 and 5. The Braga method (Eq. 10) has a different integral domain than that assumed in Eq. 1, since it assumes a uniform disk detection laser profile rather than the Gaussian type profile assumed in Eq. 1. However, if we replace the uniform disk detection laser profile in Eq. 1 with

$$q[\epsilon I_{r_n}(x,y)] = \begin{cases} \dfrac{1}{\pi r_n^2 C_i}, & \text{if } x^2 + y^2 \le r_n^2 \\ 0, & \text{otherwise} \end{cases},$$

then we see that the Braga method (Eq. 10) is a special case of Eq. 1 with a Gaussian initial postbleach profile and a uniform disk laser. By solving the integral in Eq. 1 for $\tau_D = r_e^2/(4D)$, Braga et al. (7) obtained a FRAP formula in explicit form as

$$\tilde{F}(t) = \frac{F_i}{2}\left(\frac{r_e^2}{r_n^2}\left[\sum_{m=1}^{\infty}\frac{(-K)^m}{m!m} \times \left\{1 - \exp\left(-\frac{r_n^2}{r_e^2}\times\frac{2m}{1+2mt/\tau_D}\right)\right\}\right] + 2\right). \qquad (11)$$

Although this formula provides a useful way to incorporate information about diffusion during the photobleach, it is in a considerably different form from the FRAP equation of Axelrod et al. (1) due to the differences in the underlying assumptions about the detection laser profiles. Therefore, we sought to generate a formula that would be more directly comparable to that of Axelrod et al., thus more closely connecting confocal and conventional FRAP analyses.

We hypothesized that if the detection laser profile in confocal FRAP can be approximated as a Gaussian, then the model of Axelrod et al. could be generalized to incorporate the effective radius from the initial postbleach profile, and thus generate a FRAP formula in the same form as the original FRAP equation (1). To take into account the diffusion of molecules during the bleach, we allow for a difference in the nominal radius (r_n) for the laser profile and the effective radius (r_e) for initial postbleach profiles as suggested previously by Braga et al. and others (6,7,9). Thus, our derivation makes the same assumptions that Axelrod et al. (1) did, except that the bleach and detection radii may differ. Assuming $r_n \le r_e$, Eq. 1–5 can be simplified explicitly by direct integration (Supporting Material B) in closed form as

$$F(t) = \frac{F_i\nu}{K^\nu}\gamma(\nu,K), \qquad (12)$$

where F_i is the prebleach fluorescence steady-state intensity, $\nu = r_e^2/(8D_e t + r_n^2)$, and $\gamma(\nu, K) = \int_0^K u^{\nu-1} e^{-u} du$, the incomplete γ-function. In a more familiar form, ν can be rewritten as

$$\nu = \left(2t/\tau_{D_e} + [r_n/r_e]^2\right)^{-1} \quad (13)$$

for a characteristic diffusion time τ_{D_e},

$$\tau_{D_e} = r_e^2/(4D_e). \quad (14)$$

K can be computed from the initial fluorescence intensity, $F(0)$, by solving

$$F(0) = \frac{F_i \nu_0}{K^{\nu_0}} \gamma(\nu_0, K), \; \nu_0 = \frac{r_e^2}{r_n^2}. \quad (15)$$

K computed by Eq. 5 could be used here. However, this value provides slightly different $F(0)$ from $F_{Data}(0)$ in many cases.

A series representation is also possible (Supporting Material C) as

$$F(t) = F_i \sum_{m=0}^{\infty} \frac{(-K)^m r_e^2}{m!\left(r_e^2 + m\left[8D_e t + r_n^2\right]\right)} = F_i \sum_{m=0}^{\infty} \frac{(-K)^m}{m!\left(1 + m\left[2t/\tau_{D_e} + (r_n/r_e)^2\right]\right)}, \quad (16)$$

where K can also be determined by Eq. 15.

Unlike the Braga equation (Eq. 11), our approach (Eqs. 12–16) leads to expressions of the same forms as in Eq. 6 (1), except that factors r_n/r_e occur. Notice that τ_{D_e} is now a function of an effective radius (Eq. 14), which is different than the conventional FRAP formulae (1). Notice also that how fast $F(t)$ recovers is determined by τ_D. Thus by this relationship, one has $D = D(r_e)$. In this way, r_e can actually be used as a parameter, and the recovery formula states that the larger the r_e, the larger the D. So in particular $D_n \leq D_e$, where D_n and D_e are diffusion coefficients obtained for the nominal and effective radius, respectively (Supporting Material E).

We note that the Braga method (Eq. 11) is identical to our new (to our knowledge) approach (Eqs. 12–16) under certain conditions. In particular, one can show that our generalization of the Axelrod formula (Eqs. 12–16) is a first-order approximation of the Braga equation. By expanding the exponential in the Braga equation and neglecting all terms >1, one obtains exactly the generalized FRAP formula (Eq. 16; see Supporting Material D for details).

Our proposed generalized FRAP formula is based on the assumption that the laser bleach profile and detection profile are both Gaussian. We therefore next test the validity of this assumption in several ways. First, we analyze the initial postbleach profile for an immobilized fluorophore. Next, we compare recovery curves calculated for a uniform and Gaussian profile. Finally, we show that under conditions where diffusion during the photobleach is significant, the assumed detection laser profile is less important than the magnitude of the effective radius r_e in determining D.

The confocal FRAP bleach profile is Gaussian for a small bleach ROI

Previous studies have shown that depending on the size of the bleach ROI, the detection laser profiles of a confocal laser scanning microscope can be approximated either by a Gaussian for small ROIs or by a uniform distribution with Gaussian edges for larger ROIs. The transition between two limiting cases has been reported to occur when the ROI radius is ~3 μm, depending on the bleaching depth (13,7,14).

The predicted initial postbleach profile for a Gaussian bleach laser profile is an exponential of a Gaussian. To confirm that our data fall in this regime, we performed FRAP on EGFP immobilized in Bis:Acrylamide gel using a 2.3-μm-diameter bleach region for 10 bleaching scans (Fig. 2 *A*). As shown in Fig. 2, *A* and *B*, no diffusion occurred during photobleaching or the postbleaching periods, indicating that EGFP was successfully immobilized in Bis:Acrylamide gel. We found that under these experimental conditions, the initial postbleach profile of EGFP in Bis:Acrylamide gel could be fit better by an exponential of a Gaussian than a uniform distribution (Fig. 2 *C*). Fig. 2 *C* also demonstrates that the area the confocal laser scans is slightly larger than the bleaching ROIs ($r = \pm r_n$: *dotted lines* in Fig. 2 *C*). For larger ROIs, however, the middle of ROIs flattened out, similar to an upside-down trapezoid with Gaussian edges (data not shown). Therefore, the initial postbleach profile is better approximated by a step function with Gaussian edges under these conditions (13,14).

FRAP data are not sensitive to the detection laser profile for rapidly diffusing molecules

We next tested whether the predicted recovery curves obtained from a Gaussian versus a uniform disk detection laser profiles are significantly different from one another for rapidly diffusing molecules using the formalism of Axelrod et al. (Eq. 6). To perform this analysis, we calculated theoretical recovery curves based on either a Gaussian laser or a uniform disk detection laser assuming a nominal bleach radius of 1 μm and $D = 50$ μm^2/s. For comparison, we performed a similar calculation assuming a much slower D, 0.1 μm^2/s, a value characteristic of membrane proteins (5). While the recovery curves for a uniform and Gaussian spot differed when $D = 0.1$ μm^2/s (Fig. 3 *A*), they were indistinguishable for $D = 50$ μm^2/s (Fig. 3 *B*). This suggests that the detection laser profile is not very important in determining the recovery curves for rapidly diffusing molecules.

We extended this analysis to compare the predictions of the equations of Axelrod et al. (Eq. 6), Braga et al. (Eq. 11), and our new formalism (Eqs. 12–16) for these same values of D and r_n ($F_0 = 0.5$). For the case of the slowly diffusing

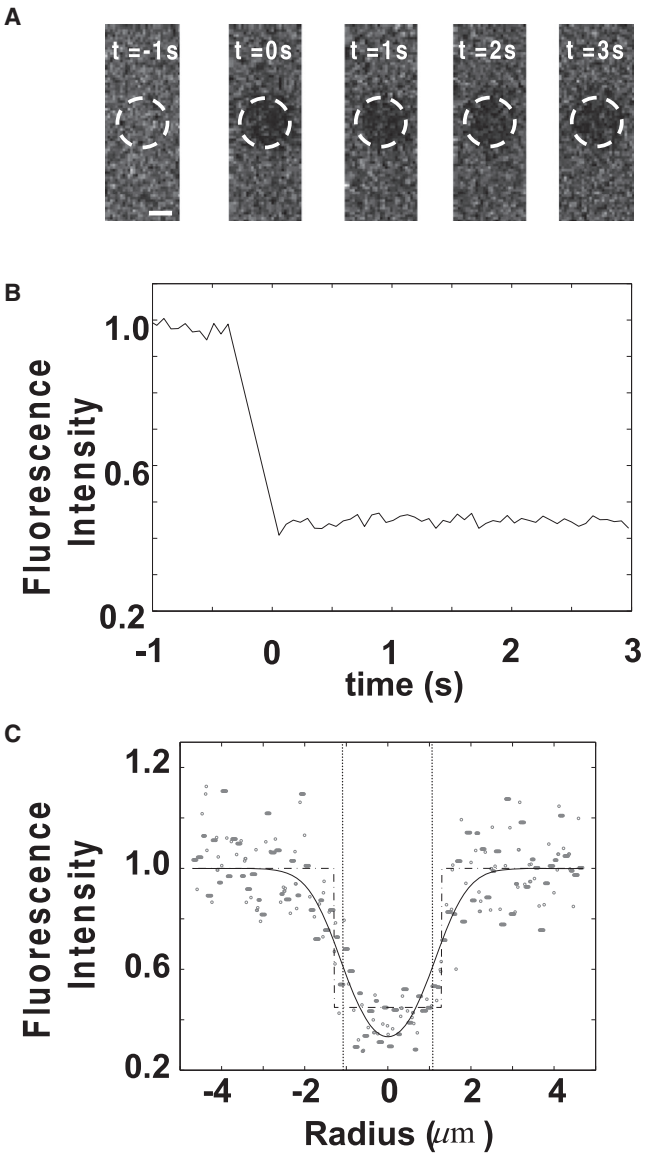

FIGURE 2 FRAP of immobilized EGFP (*A*) FRAP images of EGFP immobilized in Bis:Acrylamide gel at t $t = -1$, 0, 1, 2, and 3 (seconds). (*B*) FRAP curves of EGFP immobilized in Bis:Acrylamide gel. (*C*) Comparison of experimental initial postbleach profile (°) with either the exponential functions of a Gaussian laser (*solid line*) or a uniform disk laser profile (*dashed line*). $r = \pm r_n$ is shown by the dotted lines. Bar = 1 μm.

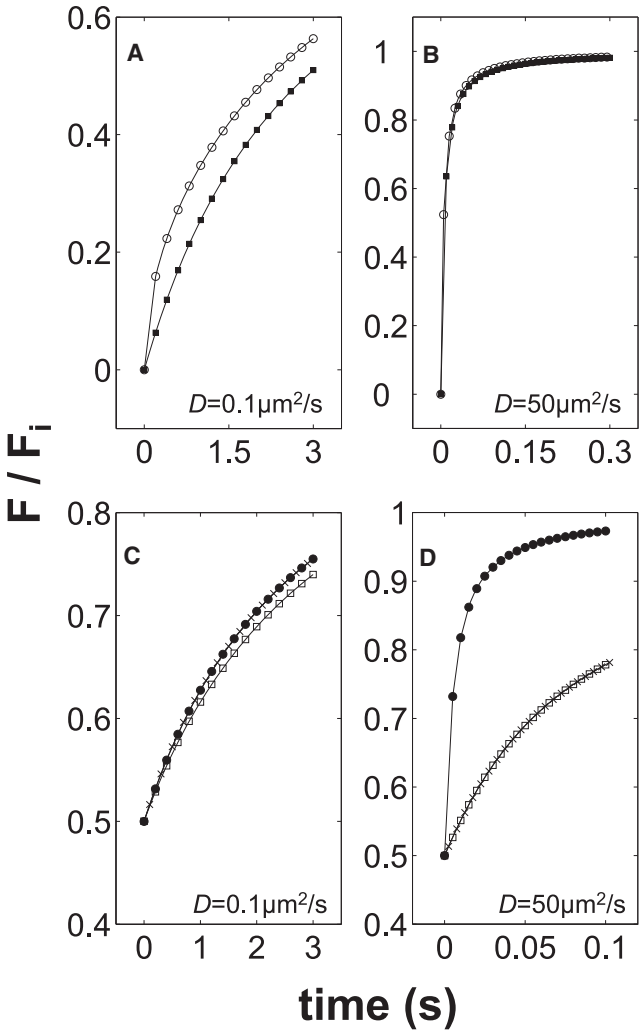

FIGURE 3 Comparison of theoretical FRAP curves from conventional and confocal FRAP equations for Gaussian and uniform disk laser profiles. (*A* and *B*) Theoretical FRAP curves calculated from the conventional FRAP formula (Eq. 6) for either a Gaussian laser profile for both photobleaching and detection profiles (■) or uniform disk laser profile for both photobleaching and detection profiles (°) assuming $r_n = r_e = 1$ μm. $D = 0.1$ μm^2/s in panel *A*, and $D = 50$ μm^2/s in panel *B*. (*C* and *D*) Theoretical FRAP curves calculated from the conventional FRAP formula for a Gaussian laser photobleaching and detection profile (Eq. 6, •), Braga's formula (Eq. 11, □) and our generalized formula (Eq. 16, ×). Pre- (F_i) and postbleach (F_0) fluorescence intensities were chosen as $F_i = 1$ and $F_0 = 0.5$, assuming full recovery ($F_\infty = F_i$). In panel *C*, $r_e = r_n = 1$ μm and $D = 0.1$ μm^2/s, and in panel *D*, $r_n = 5$ μm, $r_e = 5$ μm, and $D = 50$ μm^2/s.

molecules ($D = 0.1$ μm^2/s), we set $r_e = r_n$, whereas for the rapidly diffusing molecules ($D = 50$ μm^2/s) r_e was set as 5 μm. We found that for $D = 0.1$ μm^2/s, the theoretical recovery curves predicted by our model were identical to those predicted by the Axelrod equation (Fig. 3 *C*), while the model of Braga et al. yielded slightly slower recoveries (Fig. 3 *C*). When $D = 50$ μm^2/s, the recovery curves predicted by the generalized FRAP formula and the Braga formula were identical (Fig. 3 *D*). This further indicates that it is legitimate to assume the detection laser profile as a Gaussian for fast-diffusing molecules. In both cases, the recovery curves appear considerably slower than the curve predicted by the Axelrod equation assuming $r = r_n$ in Eq. 6. Indeed, if these curves (Fig. 3 *D*) are fit with Eq. 6, an apparent D of 3.7 μm^2/s is obtained. This is in agreement with the experimentally observed underestimation of D using the Axelrod formula under conditions where $r_n \ll r_e$.

Application of the new FRAP formula to measurements of EGFP diffusion in cells

We next applied the new FRAP formula (Eqs. 12–16) to our confocal FRAP measurements of EGFP in cells (Fig. 4) to

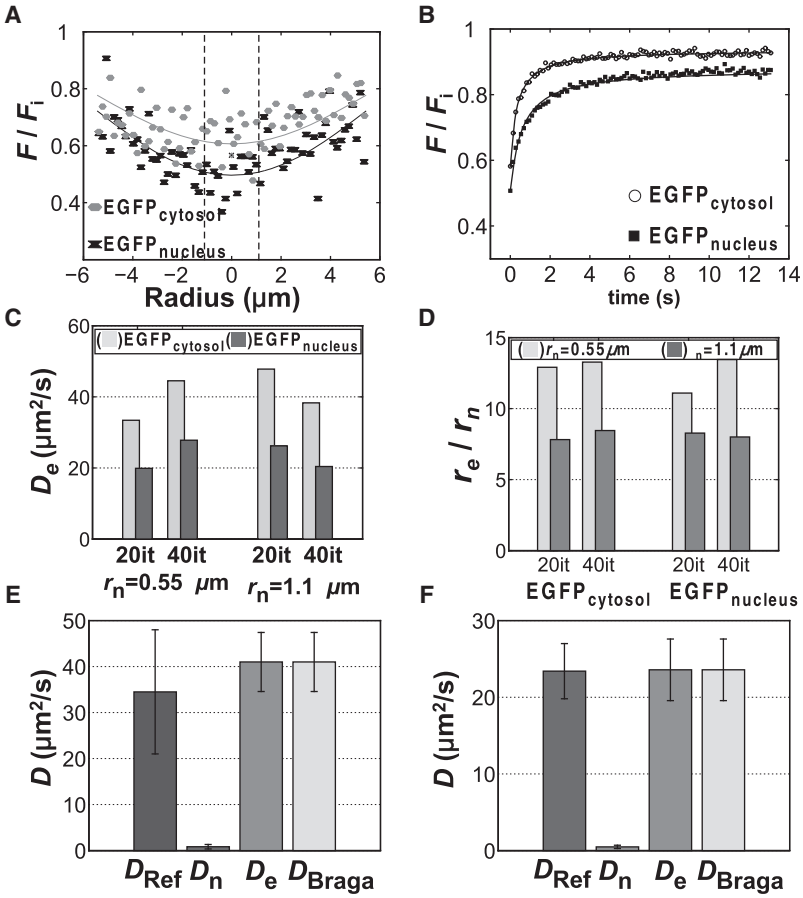

FIGURE 4 Diffusion coefficients for EGFP in the cytoplasm and the nucleus calculated using the generalized FRAP formula. (*A*) Effective radii for EGFP in the cytosol (*shading*) and the nucleus (*solid*) of COS7 cells as measured by confocal FRAP ($r_n = 1.1$ μm with 40 bleaching scan iterations). The best fits to Eq. 8 are shown as solid lines. (*B*) Comparison of confocal FRAP data for EGFP in the cytosol and the nucleus as well as the best fits to Eq. 12–16. (*C*) Dependence of D_e on experimental parameters for EGFP in the cytosol and the nucleus. (*D*) The ratio of r_e/r_n for different bleach ROI sizes and bleach scan iterations. (*E* and *F*) Comparison of *D*-values of EGFP, respectively, in either the cytosol or the nucleus of eukaryotic cells reported in the literature (15–19,7,20–22) (D_{Ref}), or measured by Eq. 4 (D_{Braga}), Eq. 12 (D_e), or conventional FRAP equation (D_n, Eq. 6). Each bar shows the mean ± SD for four different combinations of FRAP setups (20 and 40 photobleaching iterations, 10 and 20 pixel bleaching ROI radii).

determine how well this new approach accounts for diffusion during the photobleach and differences in experimental setups. For comparison, we also analyzed the data using the approach of Braga et al. (Eq. 11).

For this analysis, we first confirmed that the initial postbleach profiles for EGFP in both the cytosol and the nucleus could be approximated as exponential functions of a Gaussian (Eq. 5, Fig. 4 *A*). Since this was the case, we next measured r_e values from the initial postbleach profiles. The r_e values were a function of both the radius of the bleach ROI and the number of bleaching scans (Supporting Material F, and Fig. 4, *A* and *D*). We also noted that the r_e values and the bleaching depths from photobleaching in the cytosol were larger and shallower than in the nucleus, which implies that diffusion of EGFP in the cytoplasm is faster than in the nucleus (Fig. 4 *A*). The FRAP curves also suggest that the recovery time in the cytoplasm is shorter than in the nucleus (Fig. 4 *B*). Finally, we calculated D_e values by fitting either our new formalism (Eqs. 12–16) or the equation of Braga et al. (Eq. 11) to the FRAP data. Both approaches gave identical results. The resulting *D*-values showed little dependence on either bleach spot size or the number of bleaching scans (Fig. 4 *C*). We measured *D* for EGFP in the cytosol as 41.0 ± 6.4 $\mu m^2/s$ (Fig. 4 *E*), and *D* for EGFP in the nucleus as 23.6 ± 4.0 $\mu m^2/s$ (Fig. 4 *F*) when we averaged the data over the different combinations of bleach radii and bleach iterations. These values are quite similar to those reported in the literature for *D* of EGFP in the cytosol (21–48 $\mu m^2/s$) and in the nucleoplasm (20–33 $\mu m^2/s$) (15–19,7,20–22).

Measurements of *D* for EGFP in solutions of known viscosity using the new FRAP equation

As indicated above, our measurements of *D* for EGFP in the cytoplasm and nucleus fall within the range of reported values. However, since the reported values of *D* for EGFP in cells vary over a considerable range across studies, it is difficult to determine a priori which value is most appropriate to choose as a standard. In addition, to evaluate the validity of various FRAP equations, a comparison across a range of *D* values would be more useful than a single measurement. Therefore, as a final test of our new formalism, we measured *D* for EGFP in a series of aqueous glycerol solutions of known viscosity and compared this to theoretical values predicted by the Stokes-Einstein equation (7,23),

$$D = \frac{k_B T}{6\pi\eta\rho}. \quad (17)$$

Here, k_B is the Boltzmann constant, T is absolute temperature, η is viscosity, and ρ is a hydrodynamic radius of

diffusing molecules. It has been shown that Eq. 17 yields a good approximation for diffusion coefficients on a confocal plane as well (7).

We chose three different aqueous glycerol solutions (40, 50, and 70% by mass) to generate solutions of known viscosity (72, 4.21, and 14.1 mPas, respectively, at 30°C/303.15 K (24)). Assuming a hydrodynamic radius $\rho = 1.7$ nm for EGFP (25), the predicted diffusion coefficients of EGFP in each of these aqueous glycerol solutions could then be obtained as

$$D_{\mathrm{EGFP}}^{40\%} = 48.0\mu\mathrm{m}^2/\mathrm{s}$$
$$D_{\mathrm{EGFP}}^{50\%} = 31.0\mu m^2/\mathrm{s}. \quad (18)$$
$$D_{\mathrm{EGFP}}^{70\%} = 9.26\mu\mathrm{m}^2/\mathrm{s}.$$

For each of the glycerol solutions, we performed experiments in which we varied the size of the bleach spot (0.55- or 1.1-μm radius) as well as the number of bleach scans (20 or 40) to evaluate how well the formula could account for variations in the experimental setup (Fig. 5). Under the conditions of these experiments, all the initial postbleach profiles could be fit better by the Gaussian laser profile than the uniform circle laser profile (Fig. 5 *B*). The faster diffusion of EGFP in solutions of lower viscosity resulted in shallower bleaching depths and larger r_e values. For example, the effective radii r_e measured at $r_n = 1.1$ μm for 40 bleaching scans were found to be 11.8, 7.6, and 6.4 μm, respectively, for the 40, 50, and 70% aqueous glycerol solutions (Supporting Material F). In addition, the r_e values also depended on the number of bleaching scans as well as the bleaching spot size. When more bleach scans or a larger bleaching ROI

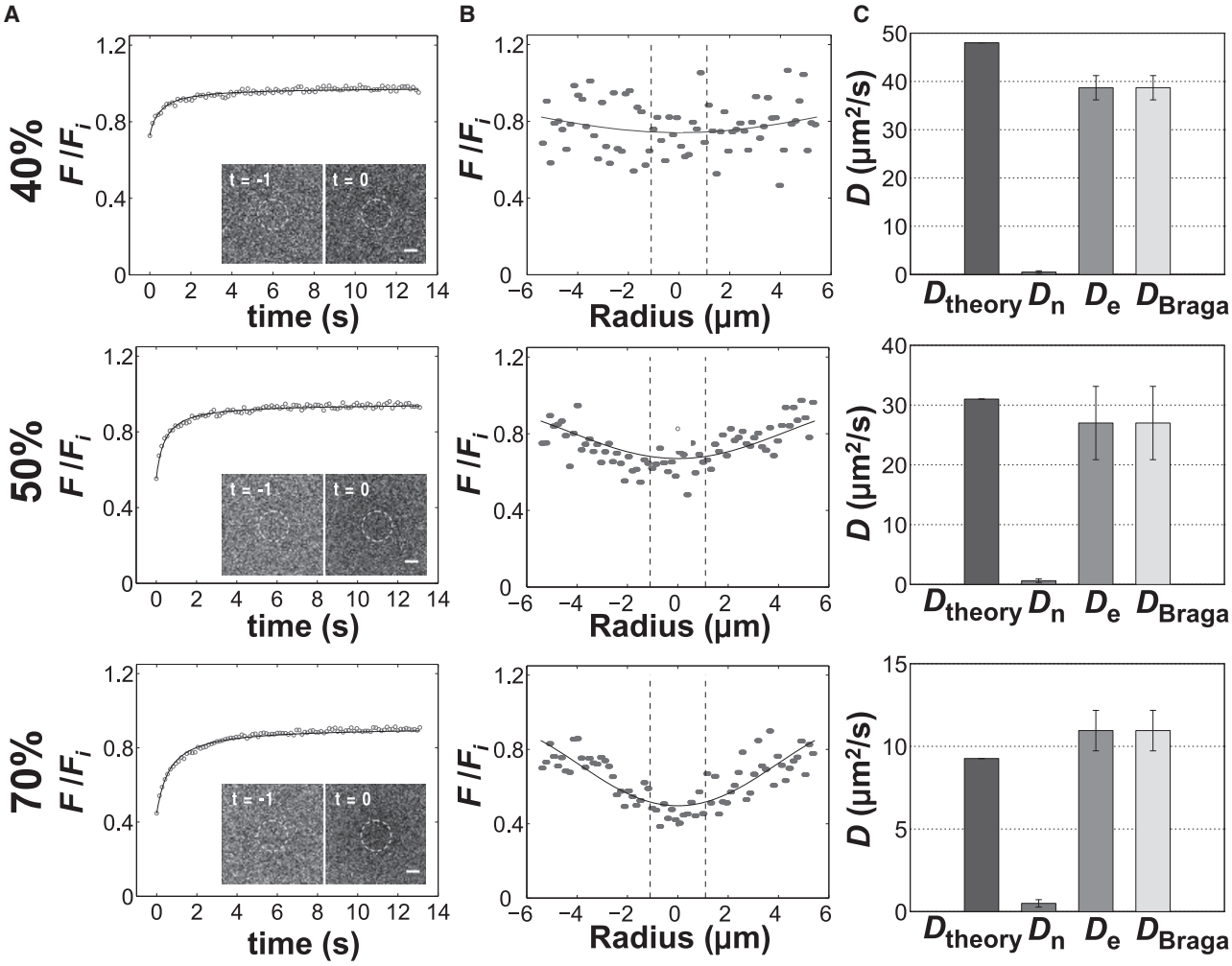

FIGURE 5 Diffusion coefficients of EGFP in aqueous glycerol solutions. Each row shows data for either 40, 50, or 70% aqueous glycerol solutions as indicated. (*A*) Normalized confocal FRAP data (°) and the best fit to Eqs. 12–16 (*solid line*) for confocal FRAP data collected using 40 photobleaching scans of a 20 pixels' radius bleach ROI. Insets show prebleach ($t = -1$) and postbleach ($t = 0$) images, where bleaching ROIs are marked as dashed circles. Scale bars are 1 μm. (*B*) Normalized fluorescence intensity distribution for the confocal FRAP data for EGFP in aqueous glycerol solutions. The shaded dots (mean for 10 measurements) were fit by Eq. 8 (*solid line*). For comparison, $r = \pm r_n$ is also shown as a dashed line. (*C*) Comparison of diffusion coefficients obtained by either Eq. 17 (D_{theory}), Eq. 11 (D_{Braga}), Eq. 16 (D_e), or conventional FRAP formula (D_n, Eq. 6). Each bar shows the mean ± SD for four different combinations of FRAP setups (20 and 40 photobleaching iterations, 10 and 20 pixel bleaching ROI radii).

size was used, a correspondingly larger value of r_e was obtained (Supporting Material F).

We next analyzed the data using the conventional FRAP equation (Eq. 6). As observed for the case of the measurements of D for EGFP in cells using the conventional FRAP equation (Fig. 4), the resulting FRAP curves fell on top of the experimental recovery curves for EGFP in solution (Fig. 5 *A*). As expected, by ignoring diffusion during photobleaching, the corresponding values of D_n were underestimated compared to the values predicted by the Stokes-Einstein equation (Fig. 5 *C*), and were also strongly dependent on the bleaching ROI size (Supporting Material F). In general, the D-values determined by applying the conventional FRAP analysis increased as the bleaching ROI sizes increased, as was reported previously (8).

Finally, we fit the FRAP data with the new FRAP formula (Eqs. 12–16) and compared this with the approach of Braga et al. (Eq. 11) using the measured r_e values (Supporting Material F). The best-fitting FRAP curves from the two approaches overlapped one another, providing identical diffusion coefficients with the same weighted residuals (Fig. 5 *A*). The resulting D-values were measured as 38.7 $\pm$ 2.5 $\mu m^2/s$, 25.9 $\pm$ 4.1 $\mu m^2/s$, and 11.0 $\pm$ 1.2 $\mu m^2/s$ ($n = 40$, Fig. 5 *C*), close to the values estimated by the Stokes-Einstein equation (Eqs. 17 and 18). Furthermore, the measured D-values were independent of either the bleaching ROI size or the number of photobleaching scans (Supporting Material F). Thus, both formalisms appear to describe FRAP data equally well under the conditions of these experiments.

DISCUSSION

Using confocal FRAP, a number of studies have reported D-values that are either much smaller than expected theoretically or that are dependent on experimental setup, presumably due to diffusion during the photobleach. To address this problem, we have derived FRAP formulae either in closed form or in series as a generalization of the Axelrod formula (1) by combining the nominal and effective radius approach and the classical FRAP formalism for circular bleach regimes. Importantly, we show that this approach yields values of D for EGFP in cells and solution that are independent of experimental setup and that are close to values predicted by the Stokes-Einstein equation. This validates the usefulness of this method in quantifying diffusion coefficients from confocal FRAP experiments.

Unlike in conventional FRAP, in confocal FRAP, it is possible to visualize the fluorescence recovery process outside of the bleach region by monitoring an area larger than the bleach region itself (Fig. 1 *A*). We took advantage of this to directly measure the initial postbleach profile. For relatively small bleach regions, we find that the initial postbleach profile is well described by an exponential of a Gaussian (Fig. 5 *B*). We also show that the effective radius r_e of the initial postbleach fluorescence intensity profile is much larger than the nominal radius r_n of the region selected for photobleaching, and that r_e depends on the size of r_n as well as the number of scans using for bleaching (Fig. 4 *D*). Because of this, if the conventional Axelrod equation is used to calculate diffusion coefficients, the resulting values of D are lower than expected and are also dependent on experimental setup.

In a previous study, an equation that corrects for diffusion during the photobleach was generated under the assumption that the bleaching laser has a Gaussian profile with effective radius r_e and a uniform disk detection profile (Eq. 11) (7). Here, we extended this approach to derive a more general equation with a form similar to that of the original Axelrod formula by making the simplifying assumption that the detection laser profile for the confocal FRAP can be approximated by a Gaussian laser profile. This assumption is supported by experimental verification that the initial postbleach profiles for EGFP in solution and in cells can be well described as an exponential of a Gaussian (Figs. 4 and 5). Furthermore, we show that in the limit of fast diffusion ($D > 10\ \mu m^2/s$), similar recovery curves are predicted theoretically for both a uniform disk laser detection profile and a Gaussian laser detection profile (Fig. 3, *A* and *B*).

We additionally demonstrated analytically that the FRAP formula presented here is a first-order approximation of that of Braga et al. (7) under certain conditions. Accordingly, FRAP analysis based on the current approach provided identical results with Braga et al. (7) for fast diffusing molecules ($D > 10\ \mu m^2/s$) (Fig. 3, *C* and *D*). However, while FRAP analysis by Braga et al. (7) and conventional FRAP analyses are limited to fast and slowly diffusing molecules, respectively (Fig. 3, *C* and *D*), our approach is applicable for both cases, interconnecting the two FRAP analyses seamlessly. Importantly, under this new theoretical framework, various tools from conventional FRAP analysis can now be easily applied to confocal FRAP. In addition, this approach can be readily incorporated into a binding diffusion model (26), as measurements of binding rate constants are also known to be affected by diffusion during the photobleach in confocal FRAP (6).

For small bleaching ROI, since even a scanning confocal bleaching laser profile can be approximated by a Gaussian function (7), the initial postbleach profile can often be approximated by an exponential of a Gaussian regardless of the mobility of fluorescent molecules. Indeed, under the conditions of our experiments we observed initial postbleach profiles that were well described as an exponential of a Gaussian (Fig. 2 *C*). However, in principle this may not always be the case (Supporting Material G). For example, for a larger bleaching ROI for slowly diffusing molecules, confocal FRAP is more likely to produce a bleach profile that is closer to a step function with Gaussian edges. Under these conditions, the choice of formalisms to fit the recovery curves depends on whether $r_e = r_n$ or $r_e > r_n$. If $r_e = r_n$, the

equation of Soumpasis can be used to obtain a diffusion coefficient (10). To our knowledge, an equation that describes the case of a uniform bleach laser and uniform detection laser for $r_e > r_n$ has not been reported. Other types of initial postbleach profiles might also occur, for example, for molecules whose diffusion is slowed due to binding interactions. In these cases, other approaches to extract diffusion coefficients may be required (27).

There are several experimental parameters that limit the applicability of our approach that depend on the time resolution of the measurement. This is determined by the time required to scan the sample, the time required to switch between bleaching and monitoring mode, and the strength of the bleaching laser (which determined how many scans are required to obtain a reasonable bleach depth). For example, under the conditions of our experiments, for very fast D-values, the initial postbleach profiles were not well defined (Fig. 5, 40% glycerol). To improve our estimates of r_e, we thus averaged data across experiments. Furthermore, depending on the exact experimental setup, we found that r_e often was relatively large, in some cases approaching 10 μm (Fig. 5). For comparison, the typical diameters of COS-7 cells range between 30 and100 μm, with a nucleus ~10 μm in diameter. Thus, r_e sometimes approached the size of either the nucleus or the cell itself (Supporting Material F). If r_e extends outside of the cell or outside of the nucleus, what does this mean, and can it be accurately measured? To address this question, we numerically simulated recoveries for two cases: 1), r_e is less than the cell size; and 2), r_e is greater than the cell size. If we write a partial differential equation that describes the photobleaching process and diffusion during photobleach, we obtain $u_t = D\Delta u - kI_{r_n}(x,y)u$, where u and k are a fluorophore concentration and a photobleaching rate, respectively, and $I_{r_n}(x,y)$ is as in Eq. 2. The numerical simulation results indicate that for r_e greater than the radius of a cell, the bleaching depth is deeper than the bleaching depth in a large cell. As a result, the fluorescence intensity at the cell boundary is lower and K is larger than the case of large cell (Supporting Material H). Nevertheless, the initial postbleach profile of two cases are similar in the neighborhood of bleaching spots, providing similar r_e values in both cases (Supporting Material H). This indicates that even for r_e greater than the radius of a cell or a nucleus, accuracy can be guaranteed by fitting the initial postbleach profile around the bleaching ROI.

The timescale of FRAP is determined by the diffusion time (τ_D). In what to our knowledge is a new approach, τ_D is a function of an effective radius ($\tau_{D_e} = r_e^2/(4D_e)$), while in the conventional FRAP equation τ_D is a function of the nominal radius ($\tau_{D_n} = r_n^2/(4D_n)$). Notice that the ratio of r_e/r_n from FRAP data decreases as r_n increases, regardless of bleaching iteration scans (Fig. 5 *D*), which indicates that r_e values become closer to r_i values as the bleaching spot size (r_n) increases. This may explain the observation that diffusion coefficients measured by confocal FRAP increase as bleaching-spot sizes increase (8). If we let D_n and D_e be diffusion coefficients obtained for the nominal and effective radius, respectively, then we have (see Supporting Material E for details)

$$D_e/D_n \simeq r_e^2/r_n^2,$$

which explains the increase in D_n measured by the conventional FRAP equation as a function of bleaching spot size.

SUPPORTING MATERIAL

Sections A–H are available at http://www.biophysj.org/biophysj/supplemental/S0006-3495(09)01122-9.

This work was supported by National Institutes of Health grants Nos. R01 GM073846 (to A.K.K.) and 1RO1GM068953-01 (to E.D.).

REFERENCES

1. Axelrod, D., D. Koppel, J. Schlessinger, E. Elson, and W. Webb. 1976. Mobility measurement by analysis of fluorescence photobleaching recovery kinetics. *Biophys. J.* 16:1055–1069.
2. Lippincott-Schwartz, J., E. Snapp, and A. Kenworthy. 2001. Studying protein dynamics in living cells. *Nat. Rev. Mol. Cell Biol.* 2: 444–456.
3. Houtsmuller, A. B. 2005. Fluorescence recovery after photobleaching: application to nuclear proteins. *Adv. Biochem. Eng. Biotechnol.* 95:177–199.
4. McNally, J. G. 2008. Quantitative FRAP in analysis of molecular binding dynamics in vivo. *Methods Cell Biol.* 85:329–351.
5. Kenworthy, A. K., B. J. Nichols, C. L. Remmert, G. M. Hendrix, M. Kumar, et al. 2004. Dynamics of putative raft-associated proteins at the cell surface. *J. Cell Biol.* 165:735–746.
6. Weiss, M. 2004. Challenges and artifacts in quantitative photobleaching experiments. *Traffic.* 5:662–671.
7. Braga, J., J. M. P. Desterro, and M. Carmo-Fonseca. 2004. Intracellular macromolecular mobility measured by fluorescence recovery after photobleaching with confocal laser scanning microscopes. *Mol. Biol. Cell.* 15:4749–4760.
8. Pucadyil, T. J., and A. Chattopadhyay. 2006. Confocal fluorescence recovery after photobleaching of green fluorescent protein in solution. *J. Fluoresc.* 16:87–94.
9. Mueller, F., P. Wach, and J. G. McNally. 2008. Evidence for a common mode of transcription factor interaction with chromatin as revealed by improved quantitative fluorescence recovery after photobleaching. *Biophys. J.* 94:3323–3339.
10. Soumpasis, D. M. 1983. Theoretical analysis of fluorescence photobleaching recovery experiments. *Biophys. J.* 41:95–97.
11. Hinow, P., C. E. Rogers, C. E. Barbieri, J. A. Pietenpol, A. K. Kenworthy, et al. 2006. The DNA binding activity of p53 displays reaction-diffusion kinetics. *Biophys. J.* 91:330–342.
12. Blonk, J., A. Don, H. V. Aalst, and J. J. Birmingham. 1993. Fluorescence photobleaching recovery in the confocal scanning light microscope. *J. Microsc.* 169:363–374.
13. Braeckmans, K., L. Peeters, N. N. Sanders, S. C. D. Smedt, and J. Demeester. 2003. Three-dimensional fluorescence recovery after photobleaching with the confocal scanning laser microscope. *Biophys. J.* 85:2240–2252.
14. Mazza, D., F. Cella, G. Vicidomini, S. Krol, and A. Diaspro. 2007. Role of three-dimensional bleach distribution in confocal and two-photon fluorescence recovery after photobleaching experiments. *Appl. Opt.* 46:7401–7411.

15. Merkle, D., D. Zheng, T. Ohrt, K. Crell, and P. Schwille. 2008. Cellular dynamics of Ku: characterization and purification of Ku-EGFP. *Chem. Bio. Chem.* 9:1251–1259.

16. Maertens, G., J. Vercammen, Z. Debyser, and Y. Engelborghs. 2005. Measuring protein-protein interactions inside living cells using single color fluorescence correlation spectroscopy. Application to human immunodeficiency virus type 1 integrase and LEDGF/p75. *FASEB J.* 19:1039–1041.

17. Goodwin, J. S., K. R. Drake, C. Rogers, L. Wright, J. Lippincott-Schwartz, et al. 2005. Depalmitoylated Ras traffics to and from the Golgi complex via a nonvesicular pathway. *J. Cell Biol.* 170:261–272.

18. Wang, Z., J. V. Shah, Z. Chen, C.-H. Sun, and M. W. Berns. 2004. Fluorescence correlation spectroscopy investigation of a GFP mutant-enhanced cyan fluorescent protein and its tubulin fusion in living cells with two-photon excitation. *J. Biomed. Opt.* 9:395–403.

19. Ruchira, M., A. Hink, L. Bosgraaf, P. J. M. van Haastert, and A. J. W. G. Visser. 2004. Pleckstrin homology domain diffusion in *Dictyostelium* cytoplasm studied using fluorescence correlation spectroscopy. *J. Biol. Chem.* 279:10013–10019.

20. Chen, Y., J. D. Müller, Q. Ruan, and E. Gratton. 2002. Molecular brightness characterization of EGFP in vivo by fluorescence fluctuation spectroscopy. *Biophys. J.* 82:133–144.

21. Dayel, M. J., E. F. Hom, and A. S. Verkman. 1999. Diffusion of green fluorescent protein in the aqueous-phase lumen of endoplasmic reticulum. *Biophys. J.* 76:2843–2851.

22. Swaminathan, R., C. P. Hoang, and A. S. Verkman. 1997. Photobleaching recovery and anisotropy decay of green fluorescent protein GFP-S65T in solution and cells: cytoplasmic viscosity probed by green fluorescent protein translational and rotational diffusion. *Biophys. J.* 72:1900–1907.

23. Gambin, Y., R. Lopez-Esparza, M. Reffay, E. Sierecki, N. S. Gov, et al. 2006. Lateral mobility of proteins in liquid membranes revisited. *Proc. Natl. Acad. Sci. USA.* 103:2098–2102.

24. Segur, J. B., and H. E. Oberstar. 1951. Viscosity of glycerol and its aqueous solutions. *Ind. Eng. Chem.* 43:2117–2120.

25. Bhattacharya, D., A. Mazumder, S. A. Miriam, and G. V. Shivashankar. 2006. EGFP-tagged core and linker histones diffuse via distinct mechanisms within living cells. *Biophys. J.* 91:2326–2336.

26. Kang, M., and A. K. Kenworthy. 2008. A closed-form analytic expression for FRAP formula for the binding diffusion model. *Biophys. J.* 95:L13–L15.

27. Beaudouin, J., F. Mora-Bermúdez, T. Klee, N. Daigle, and J. Ellenberg. 2006. Dissecting the contribution of diffusion and interactions to the mobility of nuclear proteins. *Biophys. J.* 90:1878–1894.